Wearable Electronics 1 (2024) 189–194

Contents lists available at ScienceDirect

Wearable Electronics

journal homepage: www.keaipublishing.com/en/journals/wearable-electronics

Nanofibrous metal oxide semiconductor for sensory face masks

Qing Ma[a], Haoyang Wang[a,*], Yunyu Sun[a,b], Jae-Hyuk Ahn[c], Binghao Wang[a,*]

[a] School of Electronic Science and Engineering, Southeast University, No. 2 Southeast University Road, Jiangning, Nanjing, Jiangsu 211189, China
[b] Anhui Key Laboratory of Spin Electron and Nanomaterials of Anhui Higher Education Institutes, School of Chemistry and Chemical Engineering, Suzhou University, Suzhou, Anhui 234000, China
[c] Department of Electronics Engineering, Chungnam National University, Daejeon, Republic of Korea

ARTICLE INFO

Keywords:
Gas sensor
Metal oxide semiconductor
Transistor
Smart face mask

ABSTRACT

Sensory face masks are designed to integrate sensors that monitor health metrics, such as breathing rate and body temperature, thereby providing continuous physiological data. However, current sensing materials are predominantly in film form. In this study, we report on the use of fibrous amorphous indium gallium zinc oxide, which offers an enlarged surface area to facilitate gas diffusion and transport into charge-carrying sites. A detailed morphological analysis and an electrical investigation of this fibrous network were conducted. By integrating this material with a wireless, miniaturised flexible circuit and mounting it on a face mask, we successfully monitored different human respiratory states in real time. This wearable face mask demonstrates the potential for promising applications in health monitoring.

1. Introduction

Room-temperature (RT) gas sensors with high sensitivity are in great demand in low-consumption Internet of Things applications, such as smart sensors, wearable devices and mobile robots. [1,2] Among them, metal oxide semiconductor-based gas sensors are featured with low manufacturing cost, high sensitivity and easy operation, and they have been extensively used in the detection of flammable, explosive, toxic and exhale gases. [3–5] To improve RT gas sensors' performance, strategies such as nanoisation, surface modification, doping, light activation and device optimisation have been developed. [6,7] For example, Li et al. fabricated aligned Nd-doped In_2O_3 nanofibres (~100 nm in diameter) using the electrospinning technique. When operated in a subthreshold region, the field-effect transistors exhibited an excellent response to acetone at RT, with high sensitivity ($S >$ 2000 % ppm^{-1}), fast response and recovery time and a low estimated detection limit (69 ppb). [8] We previously fabricated indium gallium zinc oxide (IGZO) nanofibres (~250 nm in diameter) using the blow-spinning technique. [9] When operated in a saturated region, the IGZO nanofibre-based field-effect transistors (FETs) performed a good linear response to NO_2, with a concentration range of 20–20 ppm. The calculated sensitivity was about 34 %/ppm, and good selectivity to NO_2 was observed. Recently, a near-infrared laser-irradiated SnO_2 film was developed to detect relative humidity from 15 % to 70 % at RT, demonstrating high sensitivity to incremental changes in relative humidity from 0.1 % to 2.2 %. [10] The sensor was also attached to a mask to detect different breathing modes. Despite these advancements, further reduction in fibre diameters for improved sensory performance remains underdeveloped, and system integration for wireless and real-time respiratory monitoring is seldom reported.

In this study, we developed ultrathin (~88 nm) amorphous IGZO nanofibres for wireless and real-time human breath monitoring. Using an electrospinning approach, IGZO nanofibres were created as the charge transport layer to enhance the surface area for gas diffusion. The resulting field-effect properties demonstrated an average mobility of 2.2 $cm^2/V{\cdot}s$ and an on/off ratio of 10^5. Moreover, we successfully recorded human breath in fast, normal and deep states, showing the sensor's fast response and recovery times and stable operation. By integrating the sensor with a flexible circuit board and mounting them on a face mask, we achieved wireless and real-time monitoring of respiratory status, highlighting its potential for practical applications in health monitoring.

2. Experimental section

2.1. Materials and nanofibre precursor solution preparation

Indium nitrate hydrate ($In(NO_3)_3{\cdot}xH_2O$), gallium nitrate hydrate ($Ga(NO_3)_3{\cdot}xH_2O$) and N, N-dimethylformamide (DMF) were purchased

Peer review under the responsibility of Editorial Board of Wearable Electronics
* Corresponding authors.
E-mail addresses: wanghaoyang@seu.edu.cn (H. Wang), binghaowang@seu.edu.cn (B. Wang).

https://doi.org/10.1016/j.wees.2024.09.001
Received 4 July 2024; Received in revised form 4 September 2024; Accepted 13 September 2024
Available online 10 October 2024

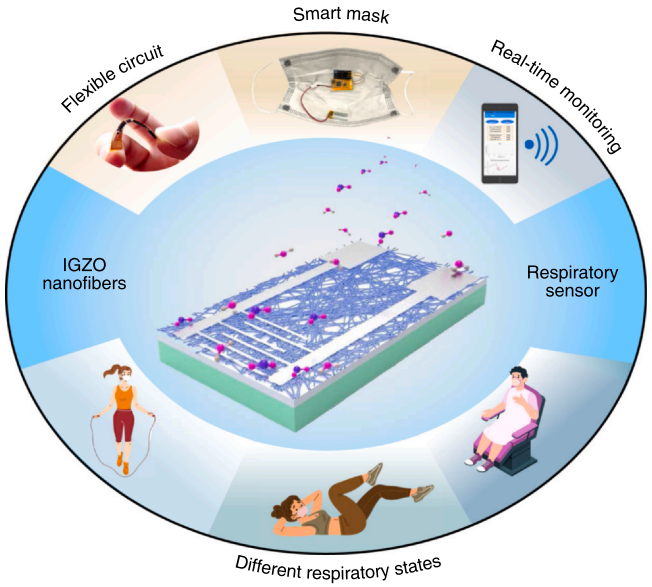

Fig. 1. Concept and design of this study: IGZO nanofibre-based sensors are integrated with a flexible circuit to create a sensory face mask, thus featuring wireless and real-time monitoring capabilities.

from Admas-Belta Ltd., China. Zinc nitrate hexahydrate ($Zn(NO_3)_2{\cdot}6\,H_2O$) and polyvinylpyrrolidone (PVP) ($M_w \sim 1300{,}000$) were bought from Sigma-Aldrich LLC. n^{++}-silicon wafers with 300 nm SiO_2 were purchased from Suzhou Resemi Co., Ltd. To fabricate IGZO nanofibres using electrospinning, PVP was added as an additive to increase the viscosity of precursor solutions. Specifically, for IGZO/PVP precursor solution preparation, 320 mg of PVP powder was dissolved in 2 mL of DMF by stirring at RT. The requisite amount of metal salt(s) [172.50 mg of $In(NO_3)_3$, 72.27 mg of $Zn(NO_3)_2$ and 75.28 mg of $Ga(NO_3)_3$] at a molar ratio of 2:1:1 was added to the PVP solution, followed by stirring for about 12 h to obtain a clear and transparent solution.

2.2. IGZO fibrous thin film and device preparations

As shown in Fig. 2a, the metal salts/PVP precursor solution was loaded into a syringe with a metal pinhead, which was fixed to a syringe pump. The gauge size of the pinhead needle was 30, with an internal diameter of 0.16 mm. A roller collector, which was used as a grounded current collector, was placed at a distance of 20 cm from the metal pinhead, and 300 nm SiO_2/Si substrates were fixed onto the collector. Electrospinning was carried out for 3 min under a positive voltage of 30 kV applied between the metal pinhead and the collector. During electrospinning, the feed rate of the precursor solution was maintained at 8 mL/h, and the rotation speed of the collector was set to 1000 RPM to obtain aligned nanofibres. The temperature and relative humidity were maintained at 20 °C and 45 %, respectively. After electrospinning, calcination was performed using tube furnace annealing from RT to 450 °C in air at a heating rate of 10 °C/min and then held at 450 °C for 100 min for IGZO/PVP nanofibres.

IGZO nanofibres-based FETs were fabricated using thermal evaporation (8×10^{-4} Pa) of the top source and drain electrodes (Al, 100 nm) through a metal shadow mask. The channel length (L) and nominal channel width (W) for all devices were 100 μm and 1000 μm, respectively. The effective W dependence on the nanofibre number/diameter was estimated optically for each device.

2.3. Nanofibre and device characterisation

The morphologies of the IGZO nanofibres were measured using a scanning electron microscope (SEM) (Helios 5 CX) and a transmission electron microscope (TEM) (Tecnai G20). The electrical measurements for the FETs were performed under ambient conditions using a Keithley 4200-SCS semiconductor parameter analyser. The electrical parameters were extracted using standard metal–oxide–semiconductor field-effect transistor equations, and carrier mobility (μ) was evaluated in the saturation region. In this study, the areal capacitance for the 300 nm SiO_2/Si substrate was 10.5 nF cm^{-2}.

According to previous studies, [1,11] the gas sensor response (R%) was calculated using equation $R\% = \Delta I/I \times 100\,\%$, where ΔI is the current change from the current under a wet air atmosphere (I_0) to the one upon the injection of gas (I). Sensitivity (S) was defined by $S = R$ %/ppb, which is the slope of the linear relationships of R% versus gas concentration.

3. Results and discussion

As illustrated in Figs. 2b and 2c, the surface morphology and microstructure of the IGZO nanofibres were evaluated by SEM and TEM, respectively. The IGZO nanofibres on the SiO_2/Si substrate exhibited a smooth and cylindrical morphology. The TEM image and selected-area electron diffraction (SAED) pattern of a single IGZO nanofibre confirmed this featureless morphology, indicating an amorphous characteristic. [9] The average diameter of the IGZO nanofibres was 88 nm, based on the statistics of more than 30 individual nanofibres, while that of electrospun metal salts/PVP fibres was 804 nm (Figs. 2d, 2e and S1). This demonstrates a significant reduction in fibre volume during thermal annealing. To evaluate their electrical performance, we fabricated FETs based on the IGZO nanofibres (Fig. 2f). The SiO_2/Si substrate served as the dielectric/gate contact, and aluminium (~100 nm thick) was thermally evaporated onto the IGZO nanofibres with a shadow mask to form the source/drain electrodes. The representative transfer and output plots are shown in Fig. 2g and S2, respectively. The transfer curve of the IGZO NF-FETs showed clear n-type semiconducting behaviour without obvious hysteresis. The on/off current ratio (I_{on}/I_{off}) could reach ~10^5, with a threshold voltage (V_T) of +20 V. Considering the average fibre diameter and number in the channel, the calculated mobilities (μ) of the IGZO NF-FETs were 2.2 cm^2 V^{-1} s^{-1}. As shown in Fig. S2, with the continuous increase in the input signal, the output current (I_{DS}) showed a decreasing trend after reaching saturation, which resulted from the depletion of available charge carriers.

Human respiratory monitoring is valuable for daily life applications, such as exercise monitoring, and medical diagnostics, including sleep apnoea detection and postoperative rehabilitation. [12,13] The primary components in exhaled breath are nitrogen (~78 %), oxygen (~16 %), carbon dioxide (4 %–5 %) and water vapor (~6 %). In addition, the temperature of exhaled breath ranges from 34 °C to 37 °C. Given that the electrical transport in IGZO nanofibres is driven by oxygen vacancies, [14] water vapor and temperature significantly affect its conductivity.

Fig. 3a shows an IGZO nanofibre-based sensor positioned near a volunteer's mouth for respiratory monitoring. When a 10 V voltage is applied, the sensor's current significantly decreases and quickly

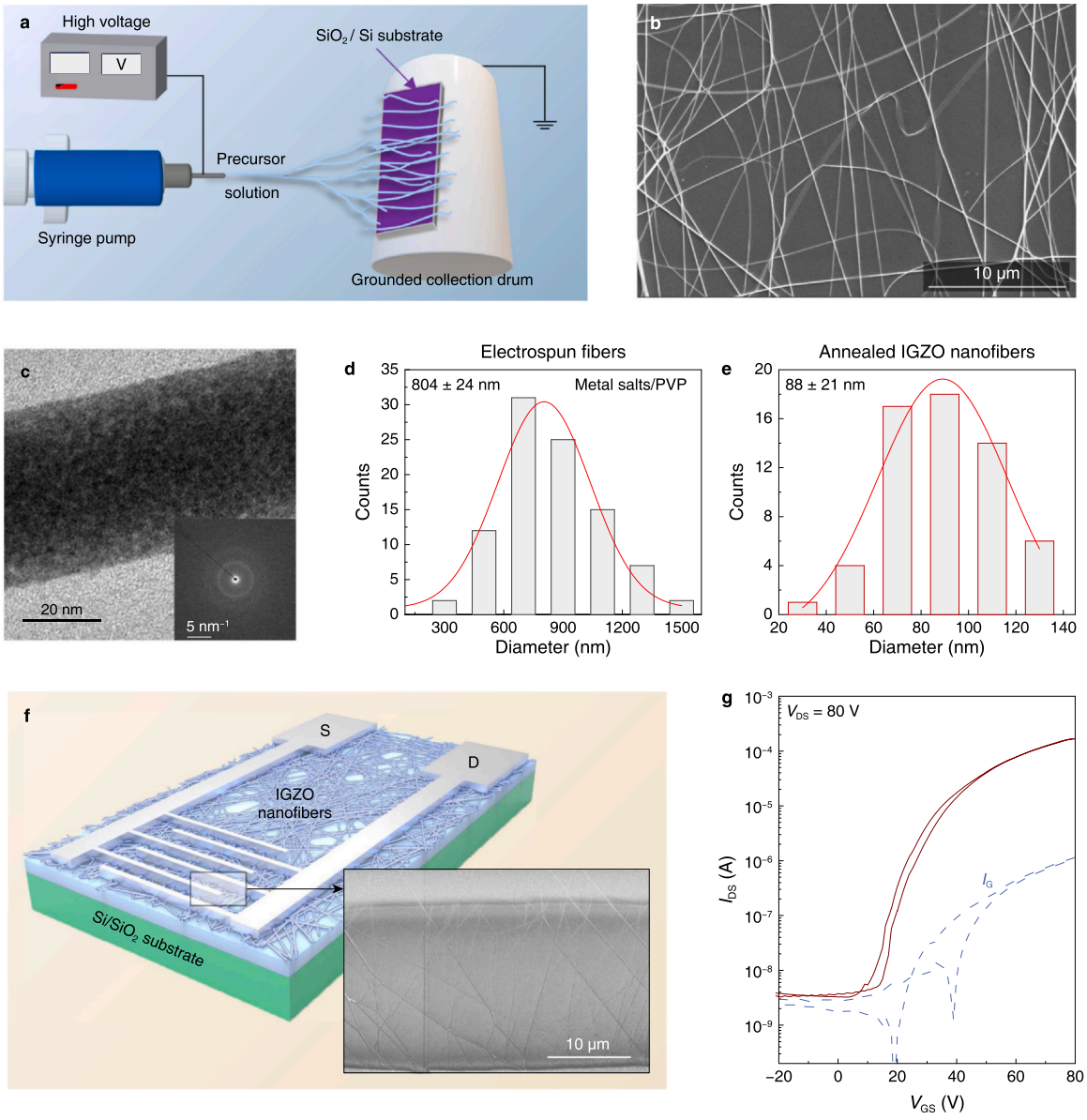

Fig. 2. Morphology and electrical characterisation of IGZO nanofibres. **a** Schematic of the electron-spinning of IGZO nanofibres. **b** SEM image of IGZO nanofibres. **c** TEM image and SAED pattern of a single IGZO nanofibre. Diameter distribution of **d** metal salts/PVP fibres and **e** annealed IGZO nanofibres. **f** Schematic of the IGZO NF-FET device structure. An inset shows the SEM image of the device. **g** Representative transfer curves of the IGZO NF-FET.

recovers during a breath cycle, with a fast response and recovery time of approximately 0.7 seconds (Fig. 3b). For adults, a typical respiration cycle lasts 3–4 seconds, although breathing frequencies vary among individuals.

To demonstrate the sensor's effectiveness, we monitored the respiratory rates of five healthy volunteers using the same sensor. As shown in Fig. 3c, the results were 18.2, 13.5, 20.0, 16.4 and 14.7 breaths per minute (bpm) for the five volunteers. The IGZO nanofibre-based gas sensor was also used to record three distinct respiratory patterns: rapid, normal and deep breathing. Fig. 3d illustrates the clear differences in respiratory rates under these different breathing patterns. The respiration rate for normal breathing was approximately 14.6 bpm, while hurried breathing reached 50.2 bpm. During deep breathing, the peak width became wider, and the rate decreased to 7.4 bpm (Fig. 3e). These findings highlight the sensor's capability to accurately monitor various respiratory patterns.

Integrating sensors into conventional face masks for monitoring human respiration presents new opportunities in personalised healthcare and pandemic prevention. [15,16] Table 1 presents recent developments in smart masks, highlighting sensor materials, types, size and monitoring methods. Key sensors include triboelectric and resistive-based pressure sensors, as well as moisture-based humidity sensors, which are known for their sensitivity and stability in detecting various respiration patterns. Less common sensors, such as thermal-based resistive and luminescence-based CO_2 sensors, have seen limited adoption. Advanced features, such as remote monitoring and high integration levels, enhance long-term usability, wearer comfort and breathability. [17,18] The most

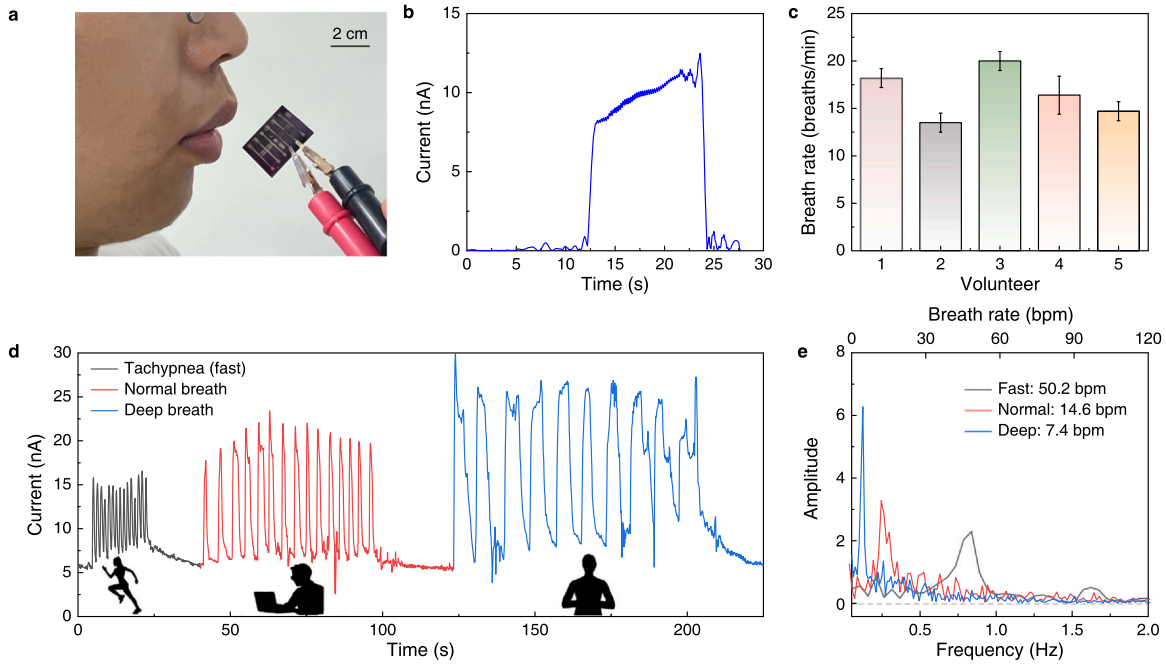

Fig. 3. Human respiratory state monitoring. **a** A photograph showing an IGZO nanofibre-based sensor for human respiration monitoring. **b** The current change when the device is exposed to breath. **c** Respiratory monitoring results of five volunteers. **d** Current recorded during normal, rapid and deep respiratory modes. **e** Breath rate and breath frequency processed using fast Fourier transform.

Table 1
Comparison of reported smart face masks.

jlv	Type	Object	Monitoring method	Size (mm^2)	Year[Ref]
LSMO[a]/Mica	Resistance	Temperature	Remote	> 50 × 50	2023 [16]
Cotton/PE[b]	TENG[c]	Airflow	Remote	> 40 × 40	2023 [19]
Silver thread	Resistance	Moisture	Local	None	2023 [20]
Graphene	Capacitance	Moisture	Local	None	2022 [21]
SnO_2	Resistance	Moisture	Local	None	2022 [22]
Graphene	Strain	Airflow	Remote	> 40 × 40	2022 [23]
Teflon/Parylene	TENG	Airflow	Remote	> 50 × 50	2022 [24]
PLA[d]/Paper	TENG	Airflow	Remote	> 100 × 50	2022 [25]
Polyaniline	Resistance	Moisture	Remote	> 100 × 100	2022 [26]
Polyester	Capacitance	Moisture	Local	None	2022 [27]
Carbon nanofibre	Resistance	Airflow	Remote	> 50 × 50	2022 [28]
Hydrogels	Resistance	Moisture	Remote	> 50 × 50	2022 [13]
Lanthanum oxysulfide	Luminescence	CO_2	Remote	45 × 60	2022 [17]
MXene	Resistance	Airflow	Remote	> 40 × 40	2021 [29]
$CsPbBr_3$	Impedance	Moisture	Local	None	2021 [30]
Cs_2TeCl_6	Resistance	Moisture	Local	None	2021 [31]
Graphene Oxide	Frequency	Moisture	Local	None	2019 [32]
IGZO nanofibre	Resistance	Moisture	Remote	15 × 35	This work

[a] $La_{0.7}Sr_{0.3}MnO_3$: LSMO;
[b] Polyethylene: PE;
[c] Triboelectric nanogenerators: TENGs;
[d] Polylactic acid: PLA

reported smart face masks with electronic components exceed the dimensions of 40 × 40 mm^2.

Furthermore, we integrated our IGZO nanofibre-based respiratory sensor with a flexible circuit for continuous real-time breath monitoring when mounted on a face mask (Figs. 4a, 4b). This sensor connects to a compact, flexible readout circuit powered by a 3.7 V battery embedded within the mask. Notably, an IGZO NF-based sensor integrated into a flexible circuit achieved a compact size of 15 × 35 mm^2, marking significant progress in the miniaturisation efforts for smart mask technology. The readout circuit, constructed on a flexible printed circuit board using standard electronic components, is illustrated in a simplified block diagram (Fig. 4c). Data collected during mask usage captured diverse respiratory states among volunteers. The recorded electrical signals can be visualised via a smartphone equipped with a customised mobile app (Figs. 4d and 4e, Video S1). It should be noted that the baseline of the respiratory curve in Fig. 4e showed a decreased baseline trend that resulted from the gathered vapor upon human exhalation.

Supplementary material related to this article can be found online at doi:10.1016/j.wees.2024.09.001.

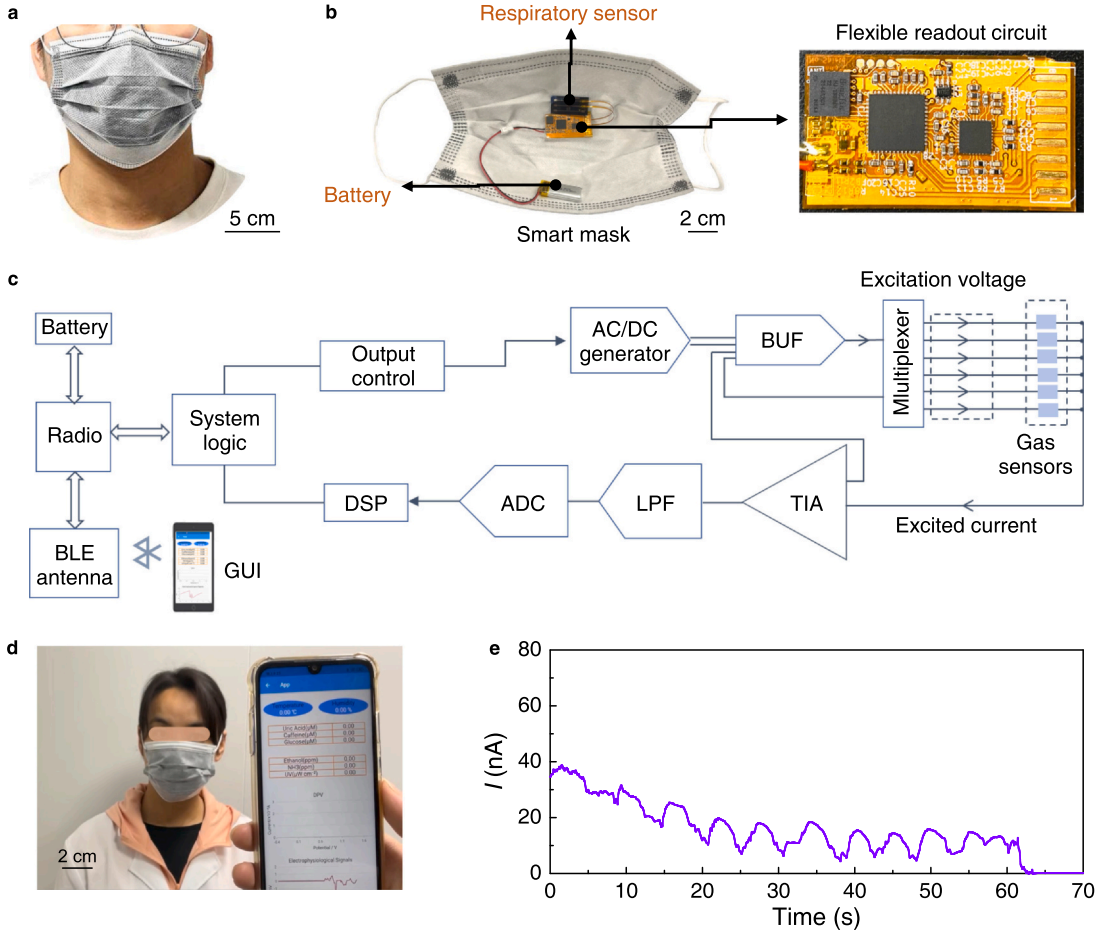

Fig. 4. Wireless sensory face mask integrated with an IGZO nanofibre sensor. **a** A photograph showing a volunteer wearing a sensory face mask. **b.** Illustration of the integrated face mask, including a wireless flexible readout circuit. **c** Detailed block diagram of the circuit. **d** Real-time respiratory monitoring using the smart face mask and **e** the corresponding response curve of the current. BUF: buffer, AC/DC: alternating current/direct current, TIA: transimpedance amplifier, LPF: low-pass filter, ADC: analogue-to-digital converter, DSP: digital signal processor, GUI: graphical user interface, and BLE: Bluetooth Low Energy.

4. Conclusion and outlook

In this study, we successfully developed a highly sensitive and selective IGZO nanofibre-based TFT gas sensor integrated into a smart mask for real-time respiration monitoring. The amorphous IGZO nanofibres, with their enhanced surface area, demonstrated superior interaction with gas molecules compared with conventional dense films. The use of IGZO nanofibre as the channel layer for TFT fabrication and the active layer for sensing endowed the device with excellent sensitivity and an immediate respiratory response. The integration of a specially designed wireless circuit and mask enabled the creation of a wireless respiratory interruption detection system with Bluetooth transmission, providing real-time monitoring of human respiration status. This advancement underscores the potential for the widespread adoption of IGZO TFT-based sensors in wearable technology, paving the way for more effective and accessible health monitoring solutions.

Ethics approval and consent to participate statements

The authors declare that the ethics approval was waived by Zhongda Hospital of Southeast University; for human breath monitoring, informed signed consent was obtained from the volunteers.

Funding

This work was supported by the National Key Research and Development Programme of China (Grant no. 2024YFE0100400), the National Natural Science Foundation of China (Grant no. 22305036), the Natural Science Foundation of Jiangsu Province (Grant no. BK20220815, BK20241291), the Science and Technology Innovation Project for Overseas Students of Nanjing grant (Grant no. 4206002301), and the Jiangsu Funding Program for Excellent Postdoctoral Talent (Grant no. 2022ZB85), and the Fundamental Research Funds for the Central Universities (Grant no. 4006002302). Y. S. would like to thank the Natural Science Research Key Project of the Education Department of Anhui Province (2022AH051377) and the Doctoral Scientific Research Foundation of Suzhou University (2021BSK008) for providing funding.

CRediT authorship contribution statement

Qing Ma: Writing – original draft, Formal analysis, Data curation. **Haoyang Wang:** Software. **Yunyu Sun:** Funding acquisition, Data curation. **Jae-Hyuk Ahn:** Writing – review & editing. **Binghao Wang:** Writing – review & editing, Supervision, Funding acquisition, Conceptualization.

Declaration of Competing Interest

The authors declare that they have no known competing financial interests or personal relationships that could have appeared to influence the work reported in this paper.

Binghao Wang is an Editorial Board Member/Guest Editor for *Wearable Electronics* and was not involved in the editorial review or the decision to publish this article.

Acknowledgement

The flexible circuit system was designed and fabricated with the assistance of Chengdu WeSys Technology Co., Ltd.

Appendix A. Supporting information

Supplementary data associated with this article can be found in the online version at doi:10.1016/j.wees.2024.09.001.

References

[1] Y. Tang, Q. Ma, J. Lu, X.Y. Jiang, L.Z. Huang, L.F. Chi, L.T. Sun, B.H. Wang, Nanofiber-textured organic semiconductor films for field-effect ammonia sensors, IEEE Open J. Nanotechnol. 3 (2022) 116–123.
[2] A. Bag, N.-E. Lee, Recent advancements in development of wearable gas sensors, Adv. Mater. Technol. 6 (2021) 2000883.
[3] L. Zhu, W. Zeng, Room-temperature gas sensing of ZnO-based gas sensor: a review, Sens. Actuator A Phys. 267 (2017) 242–261.
[4] M.T. Vijjapu, S.G. Surya, S. Yuvaraja, X.X. Zhang, H.N. Alshareef, K.N. Salama, Fully integrated indium gallium zinc oxide NO2 gas detector, ACS Sens 5 (2020) 984–993.
[5] P.F. Song, T.Q. Wang, Application of polyoxometalates in chemiresistive gas sensors: a review, ACS Sens 7 (2022) 3634–3643.
[6] J. Zhang, X. Liu, G. Neri, N. Pinna, Nanostructured materials for room-temperature gas sensors, Adv. Mater. 28 (2016) 795–831.
[7] L.X. Ou, M.Y. Liu, L.Y. Zhu, D.W. Zhang, H.L. Lu, Recent progress on flexible room-temperature gas sensors based on metal oxide semiconductor, Nanomicro. Lett. 14 (2022) 206.
[8] J. Li, L. Li, Q. Chen, W. Zhu, J. Zhang, Ultrasensitive room-temperature acetone gas sensors employing green-solvent-processed aligned inndo nanofiber field-effect transistors, J. Mater. Chem. C. 10 (2022) 860–869.
[9] B.H. Wang, A. Thukral, Z.Q. Xie, L.M. Liu, X.N. Zhang, W. Huang, X.G. Yu, C.J. Yu, T.J. Marks, A. Facchetti, Flexible and stretchable metal oxide nanofiber networks for multimodal and monolithically integrated wearable electronics, Nat. Commun. 11 (2020) 2405.
[10] M. Deb, M.Y. Chen, P.Y. Chang, P.H. Li, M.J. Chan, Y.C. Tian, P.H. Yeh, O. Soppera, H.W. Zan, SnO2-based ultra-flexible humidity/respiratory sensor for analysis of human breath, Biosensors 13 (2023) 81.
[11] S.R. Xue, S.C. Cao, Z.L. Huang, D.G. Yang, G.Q. Zhang, Improving gas-sensing performance based on MOS nanomaterials: A review, Materials 14 (2021) 4263.
[12] G. Chen, R. Guan, M. Shi, X. Dai, H. Li, N. Zhou, D. Chen, H. Mao, A nanoforest-based humidity sensor for respiration monitoring, Microsyst. Nanoeng. 8 (2022) 44.
[13] Y. Liang, Q. Ding, H. Wang, Z. Wu, J. Li, Z. Li, K. Tao, X. Gui, J. Wu, Humidity sensing of stretchable and transparent hydrogel films for wireless respiration monitoring, Nanomicro. Lett. 14 (2022) 183.
[14] J.W. Hennek, J. Smith, A. Yan, M.G. Kim, W. Zhao, V.P. Dravid, A. Facchetti, T.J. Marks, Oxygen "getter" effects on microstructure and carrier transport in low temperature combustion-processed a-InXZnO (X = Ga, Sc, Y, La) transistors, J. Am. Chem. Soc. 135 (2013) 10729–10741.
[15] Y.N. Xiao, H. Li, C. Wang, S. Pan, J.M. He, A. Liu, J. Wang, P. Sun, F.M. Liu, G.Y. Lu, Room temperature wearable gas sensors for fabrication and applications, Adv. Sens. Res. 3 (2024) 2300035.
[16] L. Ye, F. Wu, R. Xu, Z. Di, J. Lu, C. Wang, A. Dong, S. Xu, L. Xue, Z. Fan, L. Xu, K. Li, D. Li, A. Kursumovic, R. Zhao, R. Tang, L. Qiu, H. Wang, J.L. MacManus-Driscoll, Q. Jing, W. Li, H. Yang, Face mask integrated with flexible and wearable manganite oxide respiration sensor, Nano Energy 112 (2023) 108460.
[17] P. Escobedo, M.D. Fernandez-Ramos, N. Lopez-Ruiz, O. Moyano-Rodriguez, A. Martinez-Olmos, I.M. Perez de Vargas-Sansalvador, M.A. Carvajal, L.F. Capitan-Vallvey, A.J. Palma, Smart facemask for wireless CO2 monitoring, Nat. Commun. 13 (2022) 72.
[18] Z. Ye, Y. Ling, M. Yang, Y. Xu, L. Zhu, Z. Yan, P.Y. Chen, A breathable, reusable, and zero-power smart face mask for wireless cough and mask-wearing monitoring, ACS Nano 16 (2022) 5874–5884.
[19] A. Vazquez-Lopez, J.S. Del Rio Saez, J. de la Vega, X. Ao, D.Y. Wang, All-fabric triboelectric nanogenerator (AF-TENG) smart face mask: Remote long-rate breathing monitoring and apnea alarm, ACS Sens 8 (2023) 1684–1692.
[20] A. Sinha, A.K. Stavrakis, M. Simic, G.M. Stojanovic, Wearable humidity sensor embroidered on a commercial face mask and its electrical properties, J. Mater. Sci. 58 (2023) 1680–1693.
[21] W.Y. Lim, C.H. Goh, K.Z. Yap, N. Ramakrishnan, One-step fabrication of paper-based inkjet-printed graphene for breath monitor sensors, Biosensors 13 (2023) 209.
[22] M. Deb, M.Y. Chen, P.Y. Chang, P.H. Li, M.J. Chan, Y.C. Tian, P.H. Yeh, O. Soppera, H.W. Zan, SnO2-based ultra-flexible humidity/respiratory sensor for analysis of human breath, Biosensors 13 (2023) 81.
[23] H.Cheraghi Bidsorkhi, N. Faramarzi, B. Ali, L.R. Ballam, A.G. D'Aloia, A. Tamburrano, M.S. Sarto, Wearable graphene-based smart face mask for real-time human respiration monitoring, Mater. Des. 230 (2023) 111970.
[24] J. Zhong, Z. Li, M. Takakuwa, D. Inoue, D. Hashizume, Z. Jiang, Y. Shi, L. Ou, M.O.G. Nayeem, S. Umezu, K. Fukuda, T. Someya, Smart face mask based on an ultrathin pressure sensor for wireless monitoring of breath conditions, Adv. Mater. 34 (2022) e2107758.
[25] K. Zhang, Z. Li, J. Zhang, D. Zhao, Y. Pi, Y. Shi, R. Wang, P. Chen, C. Li, G. Chen, I.M. Lei, J. Zhong, Biodegradable smart face masks for machine learning-assisted chronic respiratory disease diagnosis, ACS Sens 7 (2022) 3135–3143.
[26] P. Srikrishnarka, R.M. Dasi, S.K. Jana, T. Ahuja, J.S. Kumar, A. Nagar, A.R. Kini, B. George, T. Pradeep, Toward continuous breath monitoring on a mobile phone using a frugal conducting cloth-based smart mask, ACS Omega 7 (2022) 42926–42938.
[27] A. Sinha, A.K. Stavrakis, M. Simic, G.M. Stojanovic, Polymer-thread-based fully textile capacitive sensor embroidered on a protective face mask for humidity detection, ACS Omega 7 (2022) 44928–44938.
[28] Z. Pang, Y. Zhao, N. Luo, D. Chen, M. Chen, Flexible pressure and temperature dual-mode sensor based on buckling carbon nanofibers for respiration pattern recognition, Sci. Rep. 12 (2022) 17434.
[29] L. Yang, H. Wang, W. Yuan, Y. Li, P. Gao, N. Tiwari, X. Chen, Z. Wang, G. Niu, H. Cheng, Wearable pressure sensors based on mxene/tissue papers for wireless human health monitoring, ACS Appl. Mater. Interfaces 13 (2021) 60531–60543.
[30] Z.L. Wu, J. Yang, X. Sun, Y.J. Wu, L. Wang, G. Meng, D.L. Kuang, X.Z. Guo, W.J. Qu, B.S. Du, C.Y. Liang, X.D. Fang, X.S. Tang, Y. He, An excellent impedance-type humidity sensor based on halide perovskite CsPbBr3 nanoparticles for human respiration monitoring, Sens. Actuators B Chem. 337 (2021) 129772.
[31] C. Pi, X. Yu, W. Chen, L. Yang, C. Wang, Z. Liu, Y. Wang, J. Qiu, B. Liu, X. Xu, A reversible and fastresponsive humidity sensor based on a lead-free Cs2TeCl6 double perovskite, Mater. Adv. 2 (2021) 1043–1049.
[32] Y.Y. Guan, X.H. Le, M.Z. Hu, W.X. Liu, J. Xie, A noninvasive method for monitoring respiratory rate of rats based on a microcantilever resonant humidity sensor, J. Micromech. Microeng. 29 (2019) 125001.